

Hard photon production from a chemically equilibrating quark-gluon plasma with finite baryon density at one loop and two loop

J. L. Long,^{1,2} Z. J. He,^{1,3,4,*} Y. G. Ma,^{1,3} and B. Liu⁵

¹Shanghai Institute of Applied Physics, Chinese Academy of Sciences, P.O. Box 800-204, Shanghai 201800, China

²Graduate School of the Chinese Academy of Sciences, Shanghai 201800, China

³CCAST (World Laboratory), P.O. Box 8730, Beijing 100080, China

⁴Research Center of Nuclear Theory of National Laboratory of Heavy Ion Accelerator, Institute of Modern Physics, Chinese Academy of Sciences, Lanzhou 730000, China

⁵Institute of High Energy Physics, Chinese Academy of Sciences, Beijing 100039, China

(Received 14 December 2004; published 20 December 2005)

We investigate hard photon production in a chemically equilibrating quark-gluons plasma with finite baryon density at one-loop and two-loop based on Jüttner distribution of partons of the system. We find that the photon yield increases obviously with increasing the initial quark chemical potential, and the photon production is dominated by early times. In addition, obvious difference between the calculated production and the one in the thermodynamic equilibrium system shows that the study of photon production in the chemically equilibrating system is very significant.

DOI: [10.1103/PhysRevC.72.064907](https://doi.org/10.1103/PhysRevC.72.064907)

PACS number(s): 12.38.Mh, 25.75.-q, 24.85.+p

I. INTRODUCTION

Since the existence of a deconfined quark-gluon plasma (QGP) in ultrarelativistic nuclear collisions was predicted, many efforts have been done to explore it. The QGP exists only for a very short time (several fm) in a small volume (about 100 fm³), a direct detection of this state of matter is impossible. Thus various indirect signatures have to be used for its detection, such as J/ψ suppression [1], strangeness enhancement [2], dilepton spectra [3–5], photon emission [6], etc.

Hard photons are a promising probe for the detection of the QGP created in ultrarelativistic heavy ion collisions. Because of the large mean-free path of photons and the dependence of photon production on the thermodynamical condition of the QGP, photons produced in the QGP carry information on the thermodynamical state at the moment of their production [7,8]. Previous authors have studied the production of hard photons in a QGP at finite temperature [7]. Assuming the formation of a QGP already at AGS and SPS energies, however, a finite chemical potential μ_q has to be considered [9], and even at RHIC energies the quark chemical potential μ_q may not be negligible as indicated by RQMD simulation ($\mu_q \approx 1 - 2T$) [10]. Recently, Hammon, Geiger and their co-workers [11, 12] have indicated that the initial QGP system produced at the RHIC energies has finite baryon density, Majumder and Gale [13] have discussed the dileptons from QGP produced at the RHIC energies at finite baryon density, and Bass and co-workers [14] have pointed out that the parton rescattering and fragmentation lead to a substantial increase in the net-baryon density at midrapidity over the density produced by initial primary parton-parton scatterings. These show that one may further study the effect of the quark chemical potential on the signature of the QGP formation. At given energy density

estimates based on lowest order perturbation theory indicate a strong suppression of the photon production at non-vanishing quark chemical potential μ_q as compared to the case $\mu_q = 0$ [15]. Traxler, Vija, and Thoma have computed the photon production rate of a QGP at finite quark chemical potential for a given temperature (also a given energy density) using the Braaten-Pisarski method [16]. In addition, Traxler, Strickland and their co-workers [6,17] have studied the photon production in a chemically equilibrating baryon-free QGP system.

In this work, we study the hard photon production in a chemically equilibrating QGP system with finite baryon density at one-loop and two-loop to reveal the effect of the quark chemical potential on the production. As pointed out in Refs. [18–21], the distribution functions of partons in a chemically equilibrating QGP system at finite baryon density can be given by Jüttner distributions $f_{q(\bar{q})} = \lambda_{q(\bar{q})} / (e^{(p \mp \mu_q)/T} + \lambda_{q(\bar{q})})$ for quarks (antiquarks) and $f_g(p) = \lambda_g / (e^{p/T} - \lambda_g)$ for gluons. When the parton fugacities λ_i are much less than unity as may happen during the early evolution of the parton system, the quantum effect may be neglected, the distributions have been approximated as Boltzmann form $f_{q(\bar{q})} = \lambda_{q(\bar{q})} e^{-(p \mp \mu_q)/T}$ [22]. However, this introduces an error of the order of 40% when the distribution approaches chemical equilibrium as mentioned in Ref. [18]. It should be stressed here that the most commonly used approximations are the factorized Fermi-Dirac distribution functions $f_{q(\bar{q})} = \lambda_{q(\bar{q})} / (e^{(p \mp \mu_q)/T} + 1)$ for quarks (antiquarks) and factorized Bose-Einstein distribution function $f_g(p) = \lambda_g / (e^{p/T} - 1)$ for gluons. As can be also seen from the discussion in Ref. [18] the calculated thermal screening mass under this approximation coincides with that from the Jüttner distribution only near $\lambda_g = 1$, however, in the intermediate region of the λ_g the deviation is quite significant. It shows that it is difficult to study the whole process of the chemical equilibration of the system based on the previous approximation distribution functions of partons. In this work, we describe the evolution and photon production of a chemically equilibrating QGP system at finite baryon

*Corresponding author. E-mail: hezejun@sinap.ac.cn

density on the basis of the Jüttner distribution function of partons. In this work, we consider hard photons from a chemically equilibrating QGP at both one-loop and two-loop level. We generalize the approach of Refs. [16,23,24] to the Jüttner distribution of partons at finite baryon density, and describe the evolution of the system according to Ref. [25].

The rest of the paper is organized as follows. Section II describes the evolution equations of the system. In Sec. III we give the photon production rate. The numerical results and discussions are given in Sec. IV. Section V is a brief summary.

II. EVOLUTION OF THE SYSTEM

A. Thermodynamic relations of the system

We first need to know the evolution of the chemically equilibrating QGP system at finite baryon density to study photon production. Below we describe the evolution of the system as done in Ref. [25]. Expanding densities of quarks (antiquarks) over quark chemical potential μ_q , we can get the baryon density of the system

$$n_{b,q} = \frac{g_q}{6\pi^2} \left[T^3 (Q_1^2 \lambda_q - \bar{Q}_1^2 \lambda_{\bar{q}}) + 2\mu_q T^2 (Q_1^1 \lambda_q + \bar{Q}_1^1 \lambda_{\bar{q}}) + T\mu_q^2 (Q_1^0 \lambda_q - \bar{Q}_1^0 \lambda_{\bar{q}}) + \frac{1}{3}\mu_q^3 \left(\frac{\lambda_q}{\lambda_q + 1} + \frac{\lambda_{\bar{q}}}{\lambda_{\bar{q}} + 1} \right) \right], \quad (1)$$

and corresponding energy density including the contribution of gluons

$$\varepsilon_{\text{QGP}} = \frac{g_q}{2\pi^2} \left[T^4 (Q_1^3 \lambda_q + \bar{Q}_1^3 \lambda_{\bar{q}}) + 3\mu_q T^3 (Q_1^2 \lambda_q - \bar{Q}_1^2 \lambda_{\bar{q}}) + 3\mu_q^2 T^2 (Q_1^1 \lambda_q + \bar{Q}_1^1 \lambda_{\bar{q}}) + T\mu_q^3 (Q_1^0 \lambda_q - \bar{Q}_1^0 \lambda_{\bar{q}}) + \frac{1}{3}\mu_q^4 \left(\frac{\lambda_q}{\lambda_q + 1} + \frac{\lambda_{\bar{q}}}{\lambda_{\bar{q}} + 1} \right) + \frac{g_g}{g_q} T^4 \lambda_g G_1^3 + \frac{2\pi B_0}{g_q} \right], \quad (2)$$

where $g_{q(\bar{q})}$ and g_g are, in turn, degeneracy factors of quarks (antiquarks) and gluons. The integral factors appearing in the expansion above

$$G_m^n = \int \frac{Z^n dZ}{(e^Z - \lambda_q)^m}, \quad \bar{Q}_m^n = \int \frac{Z^n dZ}{(\lambda_{\bar{q}} + e^Z)^m} \quad (3)$$

are easily calculated, numerically.

B. Evolution equation of the system

We consider the reactions leading to chemical equilibrium $gg \rightleftharpoons ggg$ and $gg \rightleftharpoons q\bar{q}$. Assuming that elastic parton scatterings are sufficiently rapid to maintain local thermal equilibrium, the evolutions of gluon and quark density can

be given by the following master equations, respectively,

$$\partial_\mu (n_g u^\mu) = R_3 n_g \left[1 - \frac{n_g}{\bar{n}_g} \right] - 2R_2^{g-q} n_g \left[1 - \left(\frac{\bar{n}_g}{n_g} \right)^2 \frac{n_q n_{\bar{q}}}{\bar{n}_q \bar{n}_{\bar{q}}} \right] \quad (4)$$

$$\partial_\mu (n_q u^\mu) = R_2^{g-q} n_g \left[1 - \left(\frac{\bar{n}_g}{n_g} \right)^2 \frac{n_q n_{\bar{q}}}{\bar{n}_q \bar{n}_{\bar{q}}} \right], \quad (5)$$

where n_i is the i particle density, and $\bar{n}_{i(\bar{i})}$ is the value of $n_{i(\bar{i})}$ at $\lambda_{i(\bar{i})} = 1$. The R_3/T and R_2^{g-q}/T are the production rates for processes $gg \rightarrow ggg$ and $gg \rightarrow q\bar{q}$ as given in Ref. [25]. We note that taking $\lambda_q = \lambda_{\bar{q}}$ does not change the qualitative property of the evolution of the system because the calculated initial quark chemical potential for Au¹⁹⁷ + Au¹⁹⁷ collisions at RHIC energies is relatively small. Combining these master equations with equations of baryon number and energy-momentum conservation

$$\partial_\mu (n_{b,q} u^\mu) = 0 \quad (6)$$

$$\frac{\partial \varepsilon_{qgp}}{\partial \tau} + \frac{\varepsilon_{qgp} + P}{\tau} = 0 \quad (7)$$

we can get evolution equations of the system on the basis of the thermodynamic relations of the system at finite baryon density as obtained above. Subsequently, we solve this set of equations to get evolutions of the temperature T , quark chemical potential μ_q and fugacities λ_q for quarks and λ_g for gluons for a set of initial conditions.

III. PHOTON PRODUCTION

We now discuss the hard photon production rate. The earlier works [6,26,27] considered the hard photon production due to annihilation $q\bar{q} \rightarrow g\gamma$ and QCD Compton ($qg \rightarrow q\gamma$ and $\bar{q}g \rightarrow \bar{q}\gamma$) scattering processes from a quark matter which appear at the one-loop level in the effective theory. Recently, it is shown by the calculations of Refs. [23,24,28–30] that significant contribution also comes from the bremsstrahlung and a new process called annihilation with scattering (AWS) that arise at two-loop level in the effective theory. At first, we consider photon production from quark annihilation $q\bar{q} \rightarrow \gamma g$ and Compton scatterings $gq \rightarrow \gamma q$ and $g\bar{q} \rightarrow \gamma \bar{q}$. Their production rates can be calculated by [26]

$$E \frac{dR}{d^3 p} = \frac{1}{2(2\pi)^8} \int \frac{d^3 p_1}{2E_1} \frac{d^3 p_2}{2E_2} \frac{d^3 p_3}{2E_3} f_1(E_1) f_2(E_2) \times (1 \pm f_3(E_3)) \delta^4(P_1 + P_2 - P_3 - K) \sum |M|^2, \quad (8)$$

where $f(E)$ is the parton distribution function, $\sum |M|^2$ the square of the matrix element for reaction processes summed over spins, colors and flavors as seen in Ref. [16]. They are

$$\sum |M|^2 = \frac{2^9 \times 5}{9} \pi^2 \alpha \alpha_s \frac{u^2 + t^2}{ut} \quad (9)$$

for the quark annihilation process, and

$$\sum |M|^2 = -\frac{2^9 \times 5}{9} \pi^2 \alpha \alpha_s \frac{s^2 + t^2}{st} \quad (10)$$

for each of the two Compton processes. $(1 \pm f_3(E_3))$ is the term which describes effects of quantum statistics in the final state. The plus sign is for the annihilation process and the minus for the two Compton processes. We follow Refs. [16,26], the rate equation can be simplified as

$$E \frac{dR}{d^3p} = \frac{1}{16(2\pi)^7 E} \int ds dt \sum |M|^2 \int dE_1 dE_2 f_1(E_1) \times f_2(E_2) [1 \pm f_3(E_1 + E_2 - E)] \times \theta(P(E_1, E_2))/(P(E_1, E_2))^{1/2}, \quad (11)$$

where $P(E_1, E_2) = -(tE_1 + (s+t)E_2)^2 + 2Es((s+t)E_2 - tE_1) - s^2E^2 + s^2t + st^2$, and θ is the step function. The letters s, t , and u are the Mandelstam variables. We insert the Jüttner distribution functions of partons

$$f_{q(\bar{q})}(p) = \frac{\lambda_{q(\bar{q})}}{e^{(p \mp \mu_{q(\bar{q})})/T} + \lambda_{q(\bar{q})}} \quad (12)$$

for quarks and antiquarks,

$$f_g(p) = \frac{\lambda_g}{e^{p/T} - \lambda_g} \quad (13)$$

for gluons, and the squared matrix elements $\sum |M|^2$ into the equation, only consider the hard part of the photon rate and replace the cutoff k_c^2 by $2m_q^2$ as done in Refs. [6,24,30]. Further following [6,7,30], we integrate over $-s + k_c^2 \leq t \leq -k_c^2$ and $2k_c^2 \leq s < \infty$. Finally, we get the photon production rates

$$\left(E \frac{dR}{d^3p}\right)_{\text{ann}} = \frac{5}{36} \frac{\alpha \alpha_s \lambda_q^2}{\pi^5 E} \int_{2k_c^2}^{\infty} ds \int_{-s+k_c^2}^{-k_c^2} dt \frac{u^2 + t^2}{ut} \times \int \frac{dE_1}{e^{(E_1 - \mu_q)/T} + \lambda_q} \frac{dE_2}{e^{(E_2 + \mu_q)/T} + \lambda_q} \times \left[1 + \frac{\lambda_g}{e^{(E_1 + E_2 - E)/T} + \lambda_g}\right] \times \theta(P(E_1, E_2))/(P(E_1, E_2))^{1/2} \quad (14)$$

for quark annihilation, and

$$\left(E \frac{dR}{d^3p}\right)_{\text{com}} = -\frac{5}{36} \frac{\alpha \alpha_s \lambda_q \lambda_g}{\pi^5 E} \int_{2k_c^2}^{\infty} ds \int_{-s+k_c^2}^{-k_c^2} dt \times \frac{u^2 + s^2}{us} \int \frac{dE_1}{e^{(E_1 \mp \mu_q)/T} + \lambda_q} \frac{dE_2}{e^{(E_2)/T} - \lambda_g} \times \left[1 - \frac{\lambda_q}{e^{(E_1 + E_2 \mp \mu_q - E)/T} + \lambda_q}\right] \times \theta(P(E_1, E_2))/(P(E_1, E_2))^{1/2} \quad (15)$$

for Compton scatterings, where α is the fine-structure constant, the running coupling constant $\alpha_s = 0.4$, the plus sign is for the Compton process $g\bar{q} \rightarrow \gamma\bar{q}$ and the minus for the Compton process $gq \rightarrow \gamma q$. For a chemically equilibrating QGP system at finite baryon density the thermal quark mass m_q^2 is given by

$$m_q^2 = \frac{4\alpha_s}{3\pi} T^2 \left[2(G_1^1 \lambda_g + Q_1^1 \lambda_q) + \left(\frac{\mu_q}{T}\right)^2 \frac{\lambda_q}{\lambda_q + 1}\right], \quad (16)$$

where G_1^1 and Q_1^1 are defined in Eq. (3).

Secondly, we consider photon production at two-loop level. Aurenche, Dutta and their co-workers [23,24] have studied the

hard photon production from the bremsstrahlung and AWS process in the framework of hard thermal loop resummed effective field theory. Especially Dutta and co-workers [24] have considered finite baryon density, although they did not include it in final calculation. In this work, we extend their expressions to estimate the photon production rates from the bremsstrahlung and AWS process at finite baryon density. Since they in the final calculation only consider the photon production from the baryon-free QGP system, the contribution from quarks is equal to the one from antiquarks. Thus they only study the contribution from quarks and multiply it by a factor 2 to get the total bremsstrahlung photon yield. However, for a QGP system at finite baryon density the contribution from quarks differs from the one from antiquarks. Thus, we should first multiply the right hand side of Eq. (43) in Ref. [24] by a factor 1/2, then add the contribution from antiquarks to get the total bremsstrahlung photon yield. In Ref. [24] the Jüttner distribution functions are defined as $f_{q(\bar{q})} = 1/(e^{(p \mp \mu_{q(\bar{q})})/T} + 1)$ for quarks (antiquarks) and $f_g = (1/e^{(p - \mu_g)/T} - 1)$ for gluons. Obviously, for fugacities $\lambda_i = e^{\mu_i}$ ($i = q, g$), these Jüttner distribution functions coincide with those given in the preceding part. Thus from Eqs. (43) and (45) of Ref. [24], we have the production rate for the bremsstrahlung process

$$\left(E \frac{dR}{d^3p}\right)_{\text{brem}} = \frac{NC_F \alpha \alpha_s}{\pi^5} (\sum e_f^2) \frac{T}{E^2} (J_T - J_L) \frac{\lambda_g}{e^{E/T} - \lambda_g} \times \int_0^{\infty} dp (p^2 + (p+E)^2) \left[\left(\frac{\lambda_q}{e^{(p - \mu_q)/T} + \lambda_q} + \frac{\lambda_q}{e^{(p + \mu_q)/T} + \lambda_q} \right) - \left(\frac{\lambda_q}{e^{(p + E - \mu_q)/T} + \lambda_q} + \frac{\lambda_q}{e^{(p + E + \mu_q)/T} + \lambda_q} \right) \right] \quad (17)$$

and for the AWS process

$$\left(E \frac{dR}{d^3p}\right)_{\text{AWS}} = \frac{NC_F \alpha \alpha_s}{\pi^5} (\sum e_f^2) \frac{T}{E^2} (J_T - J_L) \frac{\lambda_g}{e^{E/T} - \lambda_g} \times \int_0^E dp (p^2 + (E-p)^2) \left[\frac{\lambda_q}{e^{(-p + \mu_q)/T} + \lambda_q} - \frac{\lambda_q}{e^{(E - p - \mu_q)/T} + \lambda_q} \right], \quad (18)$$

where e_f is the electric charge of the quark flavor f in units of electron charge. In Eq. (18), the p -integral is carried out from 0 to E as phase space is restricted in the range $0 \leq p \leq E$. The $J_{T,L}$ integrals have been given in Refs. [23,24]. As done in Ref. [24], using asymptotic thermal quark mass $M_\infty^2 = 2m_q^2$, and thermal gluon mass

$$m_g^2 = \frac{4\alpha_s}{3\pi} T^2 \left\{ 6G_1^1 \lambda_g + N_f \left[2Q_1^1 \lambda_q + \left(\frac{\mu_q}{T}\right)^2 \frac{\lambda_q}{\lambda_q + 1} \right] \right\} \quad (19)$$

we have calculated factors J_T and J_L [24,31]. In this work, we take the quark flavor $N_f = 2.5$.

We integrate photon production rates over the space-time volume of the reaction. For the longitudinal scaling expansion

of Bjorken we obtain the volume element of the system $d^4x = d^2x_T dy d\tau$, where τ is the evolution time of the system and y the rapidity of the fluid element. We consider central collisions of $\text{Au}^{197} + \text{Au}^{197}$ so the integration over transverse coordinates just yields a factor of $d^2x_T = \pi R_A^2$, where R_A is the nuclear radius. Finally we obtain the photon spectra

$$E \frac{dn}{d^3pd^4x} = \pi R_A^2 \int_{\tau_0}^{\tau_{fin}} E \frac{dn}{d^3pd^4x} \tau d\tau, \quad (20)$$

where the thermalized matter is produced at time τ_0 , τ_{fin} the evolution time of the QGP system to the phase boundary from initial state at τ_0 .

IV. CALCULATED RESULTS AND DISCUSSIONS

A. Evolution of the system

Firstly we solve the set of evolution equations to obtain the evolutions of the temperature, quark chemical potential and fugacities λ_g and λ_q . We focus on discussion $\text{Au}^{197} + \text{Au}^{197}$ central collisions at the RHIC energies. In order to understand the effect of finite baryon density on photon production, we extend our calculation up to the initial quark chemical potential 0.852 GeV. With the help of results of the Hijing model [18], we have defined initial values as $\mu_{q0} = 0.000, 0.284, 0.568, \text{ and } 0.852$ GeV, $T_0 = 0.570$ GeV, $\lambda_{g0} = 0.08, \lambda_{q0} = 0.02$. The calculated evolution paths of the system in the phase diagram have been shown in Fig. 1. The dash-dotted, dotted, dashed, and solid lines are, in turn, the evolution paths for initial quark chemical potentials $\mu_{q0} = 0.000, 0.284, 0.568, \text{ and } 0.852$ GeV,

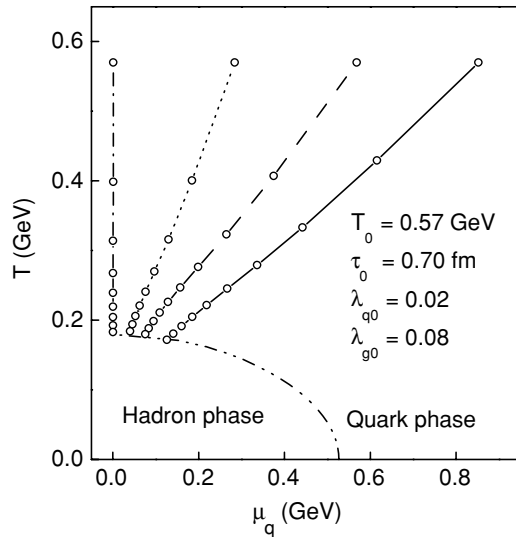


FIG. 1. The phase diagram is calculated from the bag model at the bag constant $B^{1/4} = 0.25$ GeV as done in Ref. [25]. The calculated evolution paths of the system in the phase diagram for initial values $\tau_0 = 0.25$ fm, $T_0 = 0.57$ GeV, $\lambda_{g0} = 0.08$, and $\lambda_{q0} = 0.02$, where the dash-dotted, dotted, dashed, and solid lines are, in turn, the evolution paths for initial quark chemical potentials $\mu_{q0} = 0.000, 0.284, 0.568, \text{ and } 0.852$ GeV, and the dot-dot-dashed line is the phase boundary of the phase diagram. The time interval between the two small circles is 0.5 fm (i.e., $50 \times$ calculation-step 0.01 fm).

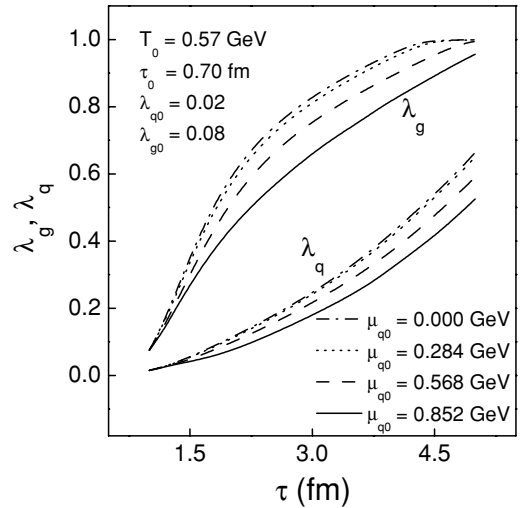


FIG. 2. The calculated equilibration rates at the same initial conditions as given in Fig. 1. The gluon and quark equilibration rates are, in turn, denoted by the λ_g and λ_q . The dash-dotted, dotted, dashed and solid lines denote, respectively, the equilibration rates for initial quark chemical potentials $\mu_{q0} = 0.000, 0.284, 0.568 \text{ and } 0.852$ GeV.

and the dot-dot-dashed line the phase boundary of the phase diagram. The time interval between the two small circles is 0.3 fm (i.e., $30 \times$ calculation-step 0.01 fm). The phase diagram is calculated at $B^{1/4} = 0.25$ GeV. We can see the effect of the finite initial quark chemical potential on the evolution of the system from Fig. 1. The increase of the initial quark chemical potential will change the hydrodynamic behavior of the system to cause the increase of the quark phase lifetime, making the evolution of the system become slower and slower towards reaching the phase boundary. In Fig. 2 we give the calculated equilibration rates at the same initial conditions as given in Fig. 1. The dash-dotted, dotted, dashed, and solid lines denote, respectively, the equilibration rates for initial quark chemical potentials $\mu_{q0} = 0.000, 0.284, 0.568, \text{ and } 0.852$ GeV. Figure 2 shows that both the chemical equilibration rates λ_g of gluons and λ_q of quarks go up rapidly with the evolution time, and that the chemical equilibration rate of gluons decreases with increasing the initial quark chemical potential.

B. Effect of finite baryon density on photon spectrum

Based on the evolution of the chemically equilibrating QGP system at finite baryon density, we calculate the photon production of the system.

The calculated photon spectra for processes $q\bar{q} \rightarrow \gamma g, gq \rightarrow \gamma q$ and $g\bar{q} \rightarrow \gamma \bar{q}$ are, in turn, shown in (a), (b), and (c) panels of Fig. 3. The calculated photon spectra for the bremsstrahlung and AWS processes are, respectively, given in (a) and (b) of Fig. 4. The total photon spectra are shown in Fig. 5. The dash-dotted, dotted, dashed, and solid lines in Figs. 3, 4, and 5 are, respectively, the calculated spectra for initial quark chemical potentials $\mu_{q0} = 0.000, 0.284, 0.568, \text{ and } 0.852$ GeV. With the increase of the quark chemical potential the antiquark density will go down, thus the photon production

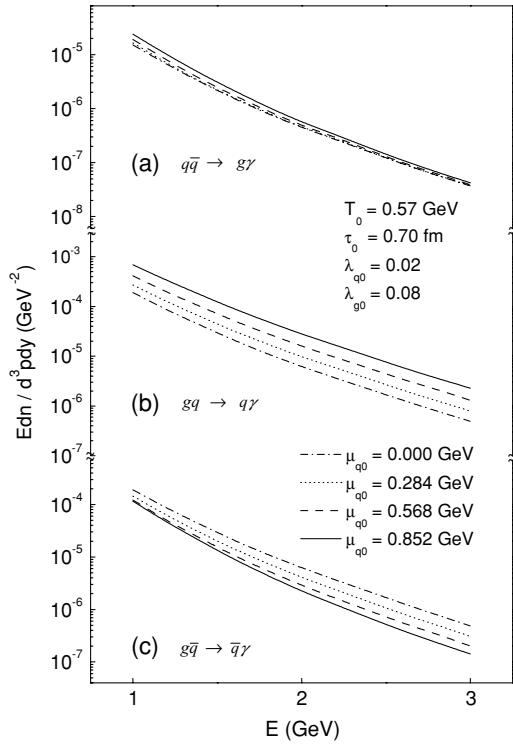


FIG. 3. The calculated photon spectra for processes $q\bar{q} \rightarrow \gamma g$, $gq \rightarrow \gamma q$, and $g\bar{q} \rightarrow \gamma \bar{q}$ are, in turn, shown in (a), (b), and (c) panels. The dash-dotted, dotted, dashed, and solid lines are, respectively, the calculated spectra for initial quark chemical potentials $\mu_{q0} = 0.000, 0.284, 0.568,$ and 0.852 GeV based on the evolution described in Fig. 1.

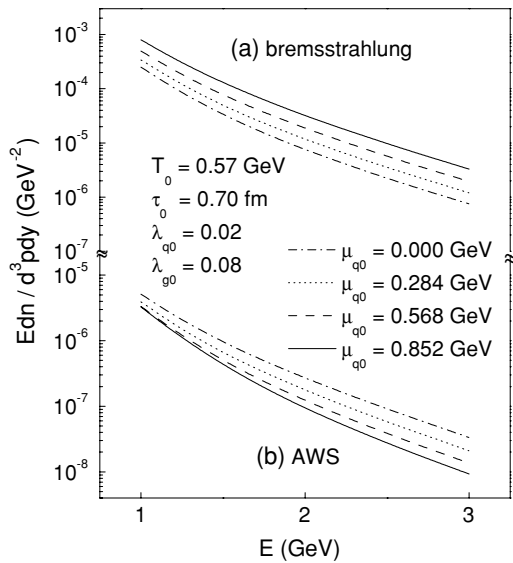


FIG. 4. The calculated photon spectra for the bremsstrahlung and annihilation with scattering processes are shown in (a) and (b). The dash-dotted, dotted, dashed, and solid lines are, respectively, the calculated spectra for initial quark chemical potentials $\mu_{q0} = 0.000, 0.284, 0.568,$ and 0.852 GeV based on the evolution described in Fig. 1.

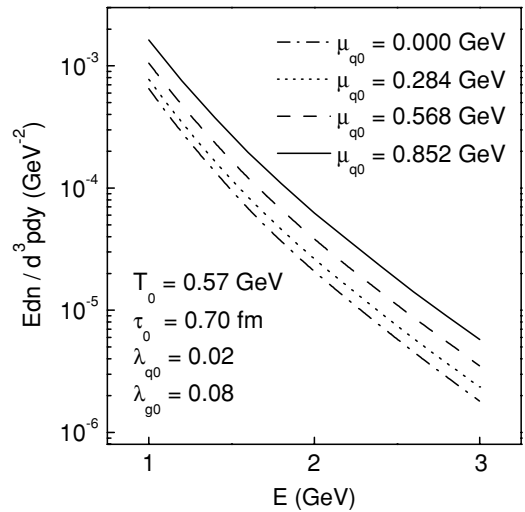


FIG. 5. The total photon spectra. The dash-dotted, dotted, dashed, and solid lines are, respectively, the calculated total photon spectra for initial quark chemical potentials $\mu_{q0} = 0.000, 0.284, 0.568,$ and 0.852 GeV based on the evolution described in Fig. 1.

for $q\bar{q} \rightarrow \gamma g$, $g\bar{q} \rightarrow \bar{q}\gamma$ and AWS process calculated from Eqs. (14), (15), and (18) will also go down. One well knows that the baryon-free QGP converts into the hadronic matter only with decreasing the temperature along the temperature axis of the phase diagram, and the phase transition occurs at a certain critical temperature T_c . However, in this work, both the quark chemical potential and the temperature of the system are functions of time, compared with the baryon-free QGP it necessarily takes a long time (also a long path) for value (μ_q, T) of the system to reach a certain point of the phase boundary to make the phase transition. Furthermore, in the calculation we have found that with increasing the initial quark chemical potential the production rate of gluons goes up, and thus the gluon equilibration rate goes down (see Fig. 2), leading to the little energy consumption of the system, i.e., slow cooling of the system. Since gluons are much more than quarks in the system, overall with increasing the initial quark chemical potential, the cooling of the system further slows down. These cause the quark phase lifetime to further increase. Such evolution features of the system can be clearly seen in Fig. 1. With the help of the calculation of Eq. (20), one can note that these factors strongly heighten the contribution of the integration over the evolution of the system to the photon production and can compensate the photon suppression. Thus the calculated spectrum for $q\bar{q} \rightarrow \gamma g$ process from Eqs. (14) and (20) go somewhat up with increasing the initial quark chemical potential, as seen in (a) of Fig. 3. It shows that the evolution of the system heightens importantly the photon production. One also knows that since with increase of the quark chemical potential the quark density goes up and antiquark density goes down, the photon production calculated by Eqs. (15) and (17) for the processes $gq \rightarrow \gamma q$ and bremsstrahlung will go up, and by Eqs. (15) and (18) for the processes $g\bar{q} \rightarrow \gamma \bar{q}$ and AWS will go down. The calculations of Eq. (20) have shown that due to the effect of the evolution of the system, with increasing the initial quark

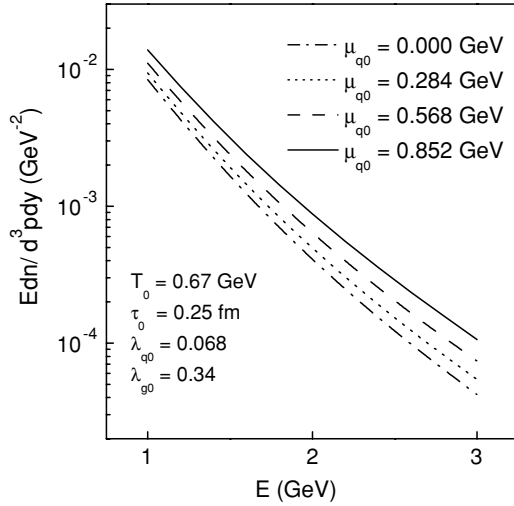


FIG. 6. The total photon spectra. The dash-dotted, dotted, dashed, and solid lines are, respectively, the calculated total photon spectra at initial quark chemical potentials $\mu_{q0} = 0.000, 0.284, 0.568,$ and 0.852 GeV for initial values $\tau_0 = 0.25$ fm, $T_0 = 0.67$ GeV, $\lambda_{g0} = 0.34,$ and $\lambda_{q0} = 0.068$ given by SSPC model calculation.

chemical potential the increase of the photon production for the processes $gq \rightarrow \gamma q$ and bremsstrahlung become even faster, and the decrease of the photon production for the processes $g\bar{q} \rightarrow \gamma \bar{q}$ and AWS obviously slows down, as seen in (c) of Fig. 3 and in (b) of Fig. 4, respectively. In the calculation, we have found that the contribution of the bremsstrahlung obviously increases with the increase of the initial quark chemical potential, and its contribution dominates, as shown in (a) of Fig. 4. This case for the baryon-free QGP has also been seen in Refs. [24,30]. Due to the bremsstrahlung and Compton process $gq \rightarrow q\gamma$, the total photon spectrum of the QGP system rises far faster with increasing the initial quark chemical potential. Finally, we can see that the total photon spectra in Fig. 5 is a strongly increasing function of the initial quark chemical potential. In Fig. 6 we also give calculated total photon spectra for initial values $\tau_0 = 0.25$ fm, $T_0 = 0.67$ GeV, $\lambda_{g0} = 0.34,$ and $\lambda_{q0} = 0.068$ which are given by SSPC model [32]. Similarly, the dash-dotted, dotted, dashed, and solid lines are, respectively, the calculated total photon spectra for initial quark chemical potentials $\mu_{q0} = 0.000, 0.284, 0.568,$ and 0.852 GeV. From Fig. 6 we can also see that the total photon spectrum increases with increasing the initial quark chemical potential.

C. Photon production as a function of evolution time

Figure 7 shows the individual contributions of different evolution time intervals to the photon spectra. The calculated photon spectra from various stages (evolution time slices) of the plasma evolution for one-loop and two-loop contributions are, respectively, plotted in (a) and (b) of Fig. 7. The calculated values in Fig. 7 are for the initial quark chemical potential $\mu_{q0} = 0.284$ GeV under the same initial conditions as given in Fig. 1. Since with the increasing of the evolution time the temperature and the quark chemical potential of the system go

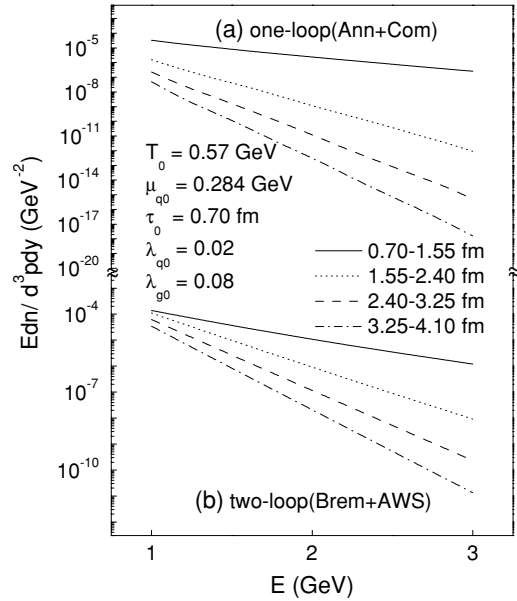


FIG. 7. The calculated photon spectra from various stages (proper time slices) of the plasma evolution for one-loop and two-loop contributions at the initial quark chemical potential $\mu_{q0} = 0.284$ GeV and the other initial values as those given in Fig. 1 are shown in (a) and (b), respectively.

down very fast and the equilibration rates rise rapidly as shown in Figs. 1 and 2, in the beginning of the evolution, the photon production calculated from Eqs. (14), (15), (17), (18), and (20) will dominate. We divide the whole evolution time into four slices, and we can see that the contributions of the earlier time slices to the photon spectra are much larger than the ones of the later time slices. While the total photon spectra at various stages (evolution time slices) of the plasma evolution under the same initial conditions as given in Fig. 7 are also shown in Fig. 8. From Figs. 7 and 8 we clearly see that the photon production are dominated by early times.

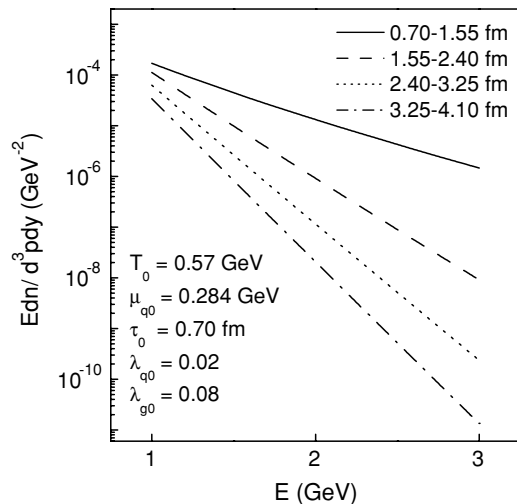


FIG. 8. The total photon spectra from various stages (proper time slices) of the plasma evolution under the same initial conditions as given in Fig. 7.

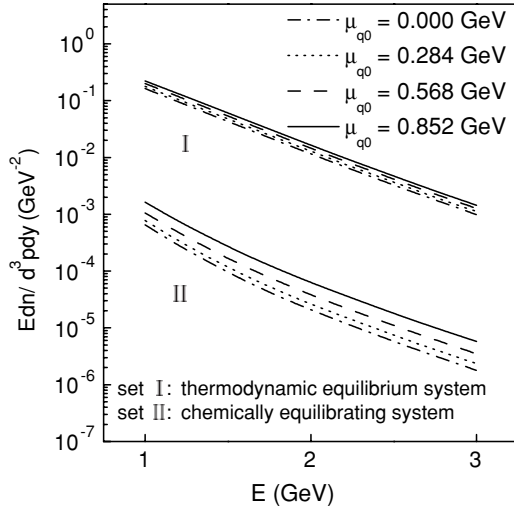


FIG. 9. The calculated photon spectra. The set I and set II of lines are, respectively, obtained from the chemically equilibrating system (based on the evolution described in Fig. 1) and the thermodynamic equilibrium system (under the initial values $\tau_0 = 0.70$ fm and $T_0 = 0.57$ GeV). The dash-dotted, dotted, dashed, and solid lines are, respectively, the calculated spectra for initial quark chemical potentials $\mu_{q0} = 0.000, 0.284, 0.568,$ and 0.852 GeV.

D. Compared with thermodynamic equilibrium system

For comparison with the results of thermodynamic equilibrium system, we have plotted the calculated photon spectra from thermodynamic equilibrium system and chemically equilibrating system in Fig. 9. The set I of lines are calculated in the thermodynamic equilibrium system ($\lambda_{q0} = \lambda_{g0} = 1$) under initial values $\tau_0 = 0.70$ fm and $T_0 = 0.57$ GeV. The set II of lines are calculated in the chemically equilibrating system for the initial values $\tau_0 = 0.70$ fm, $T_0 = 0.57$ GeV, $\lambda_{q0} = 0.02$, and $\lambda_{g0} = 0.08$ based on the evolution described in Fig. 1. The dash-dotted, dotted, dashed, and solid lines denote, respectively, the calculated spectra for initial quark chemical potentials $\mu_{q0} = 0.000, 0.284, 0.568,$ and 0.852 GeV. From Fig. 9 we have found that compared to the results from thermodynamic equilibrium system the photon production from the chemically equilibrating system is suppressed by about a factor of 10^{-2} . From Eq. (14), (15), (17), (18), and (20) one sees that the photon production rates are directly proportional to λ_q^2 or $\lambda_q \lambda_g$. Since in the thermodynamic equilibrium system the equilibration rate has reached its maximum, obviously the photon production should be larger than the one in the chemically equilibrating system. This large difference may imply that we should study the photon production in the chemically equilibrating QGP system.

V. SUMMARY

In this paper, we have studied the photon production in the chemically equilibrating QGP system at finite baryon density. We have solved the set of equations, which is

established based on the Jüttner distribution function of partons of the system, under initial values obtained by the HIJING model to get the evolution of the system. While we have also obtained the expressions of the photon production for the quark annihilation, Compton scattering, bremsstrahlung, and AWS processes via generalizing those expressions in Refs. [7,16,23,24] to describe the Jüttner distribution system. Subsequently, we have computed the photon production in a chemically equilibrating QGP system at finite baryon density, produced from Au¹⁹⁷+Au¹⁹⁷ central collisions at the RHIC energies. We find that the increase of the initial quark chemical potential will change the hydrodynamic behavior of the system to cause the quark phase lifetime to increase. This effect is to heighten the photon yield of the Compton ($gq \rightarrow q\gamma$ and $g\bar{q} \rightarrow \bar{q}\gamma$), annihilation $q\bar{q} \rightarrow g\gamma$, bremsstrahlung, and AWS process, and can compensate the photon suppression effect of processes $g\bar{q} \rightarrow \bar{q}\gamma$, $q\bar{q} \rightarrow g\gamma$, and AWS caused by the increase of the initial quark chemical potential, making the total photon yield as a strongly increasing function of the initial quark chemical potential. We also note that the bremsstrahlung process provide a dominant contribution to the photon production under the present initial conditions, and the contribution of the Compton process $gq \rightarrow g\gamma$ is very important, too. It is shown that the bremsstrahlung and Compton $gq \rightarrow g\gamma$ are two main processes making the total photon yield as a strongly increasing function of the initial quark chemical potential. Through calculating the individual contributions of different evolution time slices to the photon production, we find that the photon spectrum is ruled by the early times of the evolution of the system. Moreover, via comparing with the results from thermodynamic equilibrium system we find that the photon production of the chemically equilibrating system is suppressed by about a factor of 10^{-2} , it shows that it is very significant to study photon production in the chemically equilibrating QGP. These three physical features of photon production, which are found in this work, may be helpful to explore the new phase plasma matter.

In this work, we have studied the evolution of a chemically equilibrating QGP system at finite baryon density based on the longitudinal scaling expansion model, neglecting the effects of the nonhomogeneous distribution of the particle in space, radial flow of the system, and higher order gluon processes. In the photon calculation, we only consider the contributions from one-loop and two-loop and disregard the contributions from higher loop diagrams as given in Refs. [28,29] which may provide important contribution.

ACKNOWLEDGMENTS

This work is supported in part by CAS knowledge Innovation Project No. KJCX2-N11, the National Natural Science Foundation of China Nos. 10405031, 10575005, 10328509, and 10135030, the Major State Basic Research Development Program in China under Contract No. G200077400.

- [1] T. Matsui and H. Satz, Phys. Lett. **B178**, 416 (1986).
- [2] J. Rafelski and B. Müller, Phys. Rev. Lett. **48**, 1066 (1982).
- [3] E. Shuryak, Phys. Rep. **80**, 71 (1980).
- [4] K. Kajantie, J. Kapusta, L. McLerran, and A. Mekjian, Phys. Rev. D **34**, 2746 (1986).
- [5] A. Dumitru, D. H. Rischke, Th. Schönfeld, L. Winkelmann, H. Stocker, and W. Greiner, Phys. Rev. Lett. **70**, 2860 (1993).
- [6] C. T. Traxler and M. H. Thoma, Phys. Rev. C **53**, 1348 (1996).
- [7] J. Kapusta, P. Lichard, and D. Seibert, Phys. Rev. D **44**, 2774 (1991).
- [8] R. C. Hwa and K. Kajantie, Phys. Rev. D **32**, 1109 (1985).
- [9] S. Nagamiya, Nucl. Phys. **A544**, 5c (1992).
- [10] A. Dumitru *et al.*, Frankfurt preprint UFTP 319/1992 (unpublished).
- [11] N. Hammon, H. Stöcker, and W. Greiner, Phys. Rev. C **61**, 014901 (1999).
- [12] K. Geiger and J. I. Kapusta, Phys. Rev. D **47**, 4905 (1993).
- [13] A. Majumder and C. Gale, Phys. Rev. D **63**, 114008 (2001).
- [14] S. A. Bass, B. Müller, and D. K. Srivastava, Phys. Rev. Lett. **91**, 052302 (2003).
- [15] A. Dumitru, D. H. Rischke, H. Stöcker, and W. Greiner, Mod. Phys. Lett. A **A8**, 1291 (1993).
- [16] C. T. Traxler, H. Vija, and M. H. Thoma, Phys. Lett. **B346**, 329 (1995).
- [17] M. Strickland, Phys. Lett. **B331**, 245 (1994).
- [18] T. S. Biró, E. vanDoorn, B. Müller, M. H. Thoma, and X. N. Wang, Phys. Rev. C **48**, 1275 (1993).
- [19] P. Levai, B. Müller, and X. N. Wang, Phys. Rev. C **51**, 3326 (1995).
- [20] T. Matsui, B. Svetitsky, and L. D. McLerran, Phys. Rev. D **34**, 783 (1986).
- [21] B. Kämpfer and O. P. Pavlenko, M. I. Gorenstein *et al.*, Z. Phys. A **353**, 71 (1995).
- [22] B. Kämpfer, O. P. Pavlenko, A. Peshier, and G. Soff, Phys. Rev. C **52**, 2704 (1995).
- [23] P. Aurenche, F. Gelis, H. Zaraket, and R. Kobes, Phys. Rev. D **58**, 085003 (1998).
- [24] D. Dutta, S. V. S. Sastry, A. K. Mohanty *et al.*, Nucl. Phys. **A710**, 415 (2002).
- [25] Z. He, J. Long, W. Jiang, Y. Ma, and B. Liu, Phys. Rev. C **68**, 024902 (2003).
- [26] J. Kapusta, P. Lichard, and D. Seibert, Phys. Rev. D **44**, 2774 (1991).
- [27] R. Baier, H. Nakkagawa, A. Neigawa, and K. Redlich, Z. Phys. C **53**, 433 (1992).
- [28] P. Arnold, G. D. Moore, and L. G. Yaffe, J. High Energy Phys. **11** (2001) 057.
- [29] P. Arnold, G. D. Moore, and L. G. Yaffe, J. High Energy Phys. **12** (2001) 09.
- [30] M. G. Mustafa and M. H. Thoma, Phys. Rev. C **62**, 014902 (2000).
- [31] P. Aurenche, F. Gelis, R. Kobes, and E. Petitgirard, Z. Phys. C **75**, 315 (1996).
- [32] K. J. Eskola, B. Müller *et al.*, Phys. Lett. **B374**, 20 (1996).